Cellular/Molecular

Precise Localization of α7 Nicotinic Acetylcholine Receptors on Glutamatergic Axon Terminals in the Rat Ventral Tegmental Area

Ian W. Jones and Susan Wonnacott
Department of Biology and Biochemistry, University of Bath, Bath BA2 7AY, United Kingdom

α7 neuronal nicotinic acetylcholine receptors (nAChRs) constitute one of the predominant nAChR subtypes in the mammalian brain. Within the ventral tegmental area (VTA), nicotine application, paired with postsynaptic stimulation, contributes to a form of long-term potentiation, an effect attributed to presynaptic α7 nAChRs on glutamatergic afferents (Mansvelder and McGehee, 2000). The aim of this study was to examine the precise subcellular distribution of α7 nAChRs in the adult rat VTA to establish whether these receptors are indeed present on glutamatergic axon terminals and to determine their relationship with cholinergic afferents. The spatial relationship between α7 nAChRs, labeled using the α7 nAChR-specific antagonist α-bungarotoxin, and the local neurochemical environment was investigated by the application of multiple labeling strategies with antibodies against tyrosine hydroxylase, vesicular glutamate transporters (VGluTs), vesicular acetylcholine transporter, and glial fibrillary acidic protein. α7 nAChRs were localized at both somatodendritic and presynaptic loci within the VTA: on subpopulations of dopaminergic and nondopaminergic neurons and glutamatergic and nonglutamatergic terminals. There was no detectable α7 nAChR expression within astrocytes in the VTA. Most α7 nAChRs were cytoplasmic (82%), and the remainder were associated with the plasma membrane. Most presynaptic receptors (75%) were on glutamatergic axon terminals, with similar levels of α-bungarotoxin binding present on both VGluT1- and VGluT2-immunoreactive boutons. Both preembedding and postembedding electron microscopy revealed that presynaptic α7 nAChRs are often located at extrasynaptic (27%) and perisynaptic (61%) loci. α7 nAChRs were not associated with cholinergic synapses, consistent with their activation by a paracrine mode of acetylcholine or choline delivery.

Key words: **presynaptic α7 nicotinic receptor; α-bungarotoxin; vesicular acetylcholine transporter; tyrosine hydroxylase; ventral tegmental area; vesicular glutamate transporter**

Introduction

The mesolimbic dopamine pathway projecting from the ventral tegmental area (VTA) mediates the reinforcing properties of drugs of abuse, as well as natural rewards (Wise and Rompre, 1989). Addictive drugs, including nicotine, activate this pathway, resulting in dopamine release in the nucleus accumbens (NAcc), whereas mesolimbic pathway lesions disrupt the self-administration of drugs (Corrigall et al., 1992; Rassnick et al., 1993; Gerrits and Van Ree, 1996). This pathway may also be important for the prediction of reward (Robbins and Everitt, 2002). Dopaminergic and GABAergic projection neurons within the VTA receive excitatory glutamatergic inputs from the prefrontal cortex, lateral dorsal, and pedunculopontine tegmental nuclei. *In vivo* microdialysis studies have suggested that systemic nicotine increases dopamine release in the NAcc by enhancing this excitatory input to the VTA via local α7 nicotinic acetylcholine receptors (nAChRs) (Schilstrom et al., 1998a,b). The demonstration that, in midbrain slice preparations, pairing presynaptic application of nicotine with postsynaptic depolarization results in NMDA receptor-dependent long-term potentiation (LTP) in VTA dopaminergic neurons (Mansvelder and McGehee, 2000) has led to the presumption that α7 nAChRs reside on glutamatergic terminals in the VTA, in which they may participate in synaptic changes that contribute to long-term enhancement of excitation of the brain reward system.

α7 nAChRs are pentameric ligand-gated cation channels distinguished by a high relative permeability to Ca^{2+} (Seguela et al., 1993; Fucile, 2004), enabling α7 nAChRs to exert diverse modulatory influences via Ca^{2+}-dependent cellular mechanisms (Dajas-Bailador and Wonnacott, 2004). α7 nAChRs have been implicated in the modulation of glutamate release in several brain regions, in addition to the VTA (Engelman and MacDermott, 2004), including the hippocampus (Gray et al., 1996), olfactory bulb (Alkondon et al., 1996), and sensory cortex (Aramakis and Metherate, 1998). In these studies, the Ca^{2+} dependence and tetrodotoxin insensitivity of nicotinic mechanisms implied that α7 nAChRs are located on glutamatergic axon terminals.

In addition to their involvement in nicotine dependence, nAChRs in the VTA may also mediate a cholinergic component of addictive behavior in response to other drugs of abuse (Schof-

Received March 30, 2004; revised Nov. 1, 2004; accepted Nov. 2, 2004.
This work was supported by Grant 066063 from the Wellcome Trust (London, UK).
Correspondence should be addressed to Prof. Susan Wonnacott, Department of Biology and Biochemistry, University of Bath, Bath BA2 7AY, UK. E-mail: bsssw@bath.ac.uk.
DOI:10.1523/JNEUROSCI.3009-04.2004
 0270-6474/04/2411244-09$15.00/0

felmeer et al., 2002; Fagen et al., 2003). Cholinergic inputs to the VTA arise from the lateral dorsal and pedunculopontine tegmental nuclei and synapse directly onto the somatodendritic membranes of local GABAergic and dopaminergic neurons (Oakman et al., 1995; Garzon et al., 1999). The elucidation of the relationship between these cholinergic terminals and presynaptic nAChRs is of key importance to understanding the mechanisms of cholinergic nicotinic signaling within the VTA, particularly because choline can also activate and/or desensitize α7 nAChRs (Alkondon et al., 1997). The specificity of current anti-α7 subunit antibodies used to localize these receptors has been questioned recently (Herber et al., 2004). Therefore, we have developed an alternative strategy, based on the α7 nAChR-specific antagonist α-bungarotoxin (αBgt), which targets assembled α7 nAChRs.

Using fluorescent, biotin, and gold conjugates of αBgt, the aims of this study were (1) to define the precise subcellular localization of α7 nAChRs in the rat VTA and (2) to examine the spatial relationship between α7 nAChRs and cholinergic and glutamatergic inputs to the VTA.

Materials and Methods

All experiments were performed under a United Kingdom Home Office license and in accordance with the regulations of the United Kingdom Animals (Scientific Procedures) Act of 1986. Efforts were made to minimize animal suffering and to use only the minimum number of animals required. All reagents were obtained from VWR International (West Chester, PA) unless stated otherwise.

Confocal microscopy. Adult male Sprague Dawley rats (300 gm; $n = 5$) were deeply anesthetized with chloral hydrate (350 mg/kg, i.p.) and perfused transcardially with 30 ml of 0.1 M phosphate buffer (PB), pH 7.4, followed by 150 ml of PB containing 4% paraformaldehyde. The rats were then decapitated, the brains were removed, and 50 μm coronal sections were collected through the VTA using a vibrating microtome (Ted Pella, Redding, CA). The sections were washed three times for 10 min each in PB and then incubated in PB containing 1% sodium borohydride for 10 min to reduce residual aldehyde groups. The sections were then washed three times for 10 min each in PBS, pH 7.4, and nonspecific binding sites were blocked by incubation in PBS containing 0.5% Triton X-100 plus 10% normal goat serum (NGS) plus 0.5% bovine serum albumin (BSA) for 1 hr. The sections were rinsed in PBS and then incubated in 10 nM fluorescent αBgt (αBgt Alexa Fluor 488; Molecular Probes, Eugene, OR) diluted in PBS containing 0.5% Triton X-100 plus 0.5% NGS overnight at 4°C. To visualize the association between αBgt binding sites and the local neurochemical environment in the VTA, two primary antibodies were added to the incubation medium. These were directed against cholinergic axon terminals [rabbit anti-vesicular acetylcholine transporter (VAChT); Chemicon, Temecula, CA], dopaminergic neurons (mouse anti-tyrosine hydroxylase; Chemicon), astrocytes [rabbit anti-glial fibrillary acidic protein (GFAP); BioGenex, San Ramon, CA], glutamatergic axon terminals [rabbit or guinea pig anti-vesicular glutamate transporter type 1 (VGluT1) or VGluT2; Synaptic Systems, Goettingen, Germany, or Chemicon, respectively], or neuronal axonal boutons (mouse anti-synaptophysin; Synaptic Systems). Antibody dilutions were as recommended by the respective supplier.

After primary antibody incubation, the sections were washed four times for 10 min each in PBS and then incubated in 10 nM fluorescent αBgt plus fluorochrome-linked secondary antibodies (Alexa Fluor 546 and 633 conjugates, made in goat and directed against respective primary antibody species), diluted 1:750 in PBS containing 0.5% Triton X-100 plus 0.5% NGS overnight at 4°C. The sections were subsequently washed four times for 10 min each in PBS, mounted on microscope slides in Vectorshield mounting medium (Vector Laboratories, Burlingame, CA), and viewed in a Zeiss (Goettingen, Germany) LSM 510 confocal microscope using multitracking protocols to prevent fluorochrome "cross talk."

Electron microscopy: unfixed slices. α7 nAChRs were localized in unfixed coronal VTA slices using either biotinylated αBgt (Molecular Probes) or 1.4 nm gold-conjugated αBgt (custom synthesized by Molecular Probes) (Jones et al., 2004). Adult male Sprague Dawley rats (300 gm; $n = 3$) were deeply anesthetized with chloral hydrate (350 mg/kg, i.p.) and perfused transcardially with 150 ml of ice-cold artificial CSF (ACSF) containing (in mM): 125 NaCl, 25 $NaHCO_3$, 2.5 KCl, 2 $CaCl_2$, 2 $MgCl_2$, 25 glucose, and 1.25 NaH_2PO_4, oxygenated with 95% O_2 and 5% CO_2 for 1 hr and then adjusted to pH 7.4. The rats were subsequently decapitated, the brains were removed, and 150 μm slices through the VTA were collected using a vibrating microtome and washed three times for 5 min each in ice-cold ACSF. The slices were allowed to reach room temperature and were then blocked in ACSF containing 0.2% acetylated BSA (ACSF–BSAc) for 30 min. The sections were rinsed briefly in ACSF and then incubated in 10 nM biotinylated or gold αBgt in ACSF–BSAc for 1 hr. The sections were washed three times for 10 min each in ACSF–BSAc and then fixed in ACSF containing 2.5% glutaraldehyde for 30 min.

Slices incubated in biotinylated αBgt were postfixed in 0.5% OsO_4 in PB for 15 min, dehydrated through an alcohol series into propylene oxide, infiltrated with Durcupan epoxy resin (Fluka, Buchs, Switzerland) overnight, and flat-embedded on microscope slides. The slices were cured in an oven at 60°C for 48 hr, and ultrathin sections (60 nm) were collected onto pioloform-coated nickel slot grids using an Ultracut E microtome (Leica Microsystems, Milton Keynes, UK). Ultrathin sections were immunolabeled for biotin using the postembedding technique described previously (Ingham, 1992). Briefly, sections were etched in 1% periodic acid for 20 min and incubated in 1% sodium metaperiodate for 20 min to remove excess osmium, and nonspecific binding sites were blocked by incubation in Tris-buffered saline (TBS) (50 mM Tris plus 0.9% NaCl, pH 7.4) containing 5% NGS for 30 min. The sections were then incubated in 10 nm gold-conjugated goat anti-biotin antibody (Aurion, Wageningen, The Netherlands), diluted 1:100 in TBS containing 1% NGS plus 0.05% polyethylene glycol (average molecular weight, 3350 Da) for 2 hr. The sections were rinsed in five changes of deionized water (DW), counterstained with uranyl acetate and lead citrate according to standard methods, and viewed in a Jeol (Peabody, MA) 1200EX transmission electron microscope (EM).

Slices incubated in gold αBgt were washed four times for 10 min each in DW and then silver-enhanced for 60 min (R-GENT SE-EM reagent; Aurion). After silver enhancement, the sections were washed four times for 10 min each in DW, postfixed in 0.5% OsO_4 in PB for 15 min, and embedded in Durcupan resin as above, and 60 nm sections were collected onto pioloform-coated nickel slot grids. The grids were counterstained with uranyl acetate and lead citrate before viewing in a Jeol 1200EX transmission electron microscope.

Electron microscopy: fixed slices. The subcellular association between α7 nAChRs and neurochemical markers, such as vesicular glutamate transporters, was addressed in fixed coronal VTA sections. α7 nAChRs were localized using either biotinylated αBgt or gold-conjugated αBgt, as described above. Briefly, adult male Sprague Dawley rats (300 gm; $n = 5$) were deeply anesthetized with chloral hydrate (350 mg/kg, i.p.) and perfused transcardially with 50 ml of 0.1 M PB, pH 7.4, followed by 200 ml of 2% paraformaldehyde, 0.1 M sodium metaperiodate, and 0.1 M L-lysine in PB, pH 7.4 (PLP fixative). The rats were then decapitated, the brains were removed and washed in PB, and 70 μm coronal sections were collected through the VTA using a vibrating microtome. The sections were rinsed three times for 10 min each in PB and incubated in 0.1% sodium borohydride in PB for 15 min to inactivate free aldehyde groups. Sections were washed four times for 10 min each in PB and then permeabilized by incubating in PB containing 0.05% Triton X-100 for 30 min. Sections were washed four times for 10 min each in PB, and then nonspecific binding sites were blocked using 10% NGS in PBS–BSAc for 30 min. Subsequently, sections were incubated in 10 nM biotinylated αBgt or gold αBgt in PBS–BSAc overnight at 4°C.

Sections were washed six times for 10 min each in PBS–BSAc and then incubated in horseradish peroxidase (HRP)-conjugated secondary antibodies (made in goat against primary antibody species; Vector Laboratories) diluted 1:1000 in PBS–BSAc for 2 hr. For experiments using biotinylated αBgt, anti-biotin 1 nm gold (diluted 1:100; Aurion) was included with the secondary antibody incubation. The sections were washed four times for 10 min each in PBS, washed two times for 10 min

each in PB, and postfixed in aldehyde in PB for 1 hr. After fixation, the sections were washed two times for 10 min each in PB, washed four times for 10 min each in DW, and silver-enhanced for 60 min. Sections were then washed four times for 10 min each in DW and two times for 10 min each in TBS, and then HRP bound to the secondary antibodies was localized by incubation with 0.005% hydrogen peroxide in the presence of 660 μM diaminobenzidine in 0.05 M Tris buffer (TB), pH 7.4. Sections were subsequently washed three times for 10 min each in TB and processed for electron microscopy, as described above.

Labeling specificity. The αBgt conjugates used in this study have been shown previously to be specific for α7 nAChRs in comparable labeling studies by competition with α7 nAChR-specific antagonists such as unconjugated αBgt and α-cobratoxin (Kawai et al., 2002; Jones et al., 2004). To confirm this specificity, these controls were repeated in each experiment by incubating samples in 100-fold excess of either unconjugated αBgt (Molecular Probes) or α-cobratoxin for 1 hr before the addition of biotinylated or gold αBgt. The specificities of the primary antibodies used have been confirmed by the respective suppliers. The specificity of the secondary antibodies was evaluated by the omission of the primary antibodies from each immunoreaction.

Data analysis. Confocal microscopy images were collected using the Zeiss multitracking protocol, which uses sequential fluorochrome excitation to eliminate the incidence of cross talk. The pinhole for each laser track was set at 1 airy unit to ensure that data were collected from the same level within the sections. To investigate the spatial relationship between the fluorescent signals, the Zeiss profiling software was used to plot fluorescence intensities along a user-defined path. For each association, a minimum of 20 random fluorescent profiles were obtained and analyzed.

For electron microscopy experiments, ultrathin sections were collected within 10 μm of the labeled section surface to ensure equal penetration of immunoreagents. Random-field micrographs (20 per sample at 7500× magnification) were used for data analyses such as gold particle counts. Because nAChRs are typically expressed at low densities in the CNS (Jones et al., 2001), structures were deemed to be αBgt-positive if they contained two or more gold particles.

Results

Confocal microscopy

Triple-labeling confocal microscopy was used to investigate the cellular distribution of α7 nAChRs within the VTA with respect to dopaminergic neurons, GFAP-immunopositive astrocytes, and glutamatergic and cholinergic axon terminals. At a low magnification (Fig. 1*A*,*B*), α7 nAChRs (identified by fluorescent αBgt binding sites) were not discernable. However, both VGluT1 (Fig. 1*A*) and VGluT2 (Fig. 1*B*) immunoreactivities were observed in the VTA, with differential labeling of the neighboring interpeduncular nucleus. At a higher magnification, αBgt binding sites were visualized in the VTA (Fig. 1*C*), and subpopulations were associated with VGluT-immunopositive structures likely to be axon terminals (yellow arrows), tyrosine hydroxylase-positive dopaminergic neurons (blue arrows), and nondopaminergic structures (green arrows). Notably, not all of the glutamatergic axonal boutons expressed αBgt binding sites (red arrows). Preincubation of the sections with an excess of unconjugated αBgt (Fig. 1*D*) or α-cobratoxin (data not shown) eliminated fluorescent αBgt labeling, demonstrating that the fluorescent αBgt binds specifically to α7 nAChRs. Sections labeled for both VGluT1 and VGluT2 isoforms, using different fluorochromes (Fig. 1*E*), showed complementary labeling of structures interpreted to be axon terminals, with no evidence of colocalization. This indicates that VGluT1 and VGluT2 are likely to be localized to separate axon terminals in the VTA.

The colocalization of α7 nAChRs with each VGluT isoform was demonstrated (Fig. 2*A–J*) and confirmed using fluorescence profiling (Fig. 2*E*,*J*). This analytical tool (see Materials and Methods) permits individual fluorescence intensities to be plotted along a user-defined line. In Figure 2, *D* and *I*, the line of analysis is represented by white arrows, and Figure 2, *E* and *J*, illustrates the respective fluorescence intensities along these paths in the direction of the arrows. In both of the representative examples shown, the αBgt signals (green peaks) overlap with the VGluT1 (Fig. 2*D*) and VGluT2 (Fig. 2*I*) signals (red peaks), in-

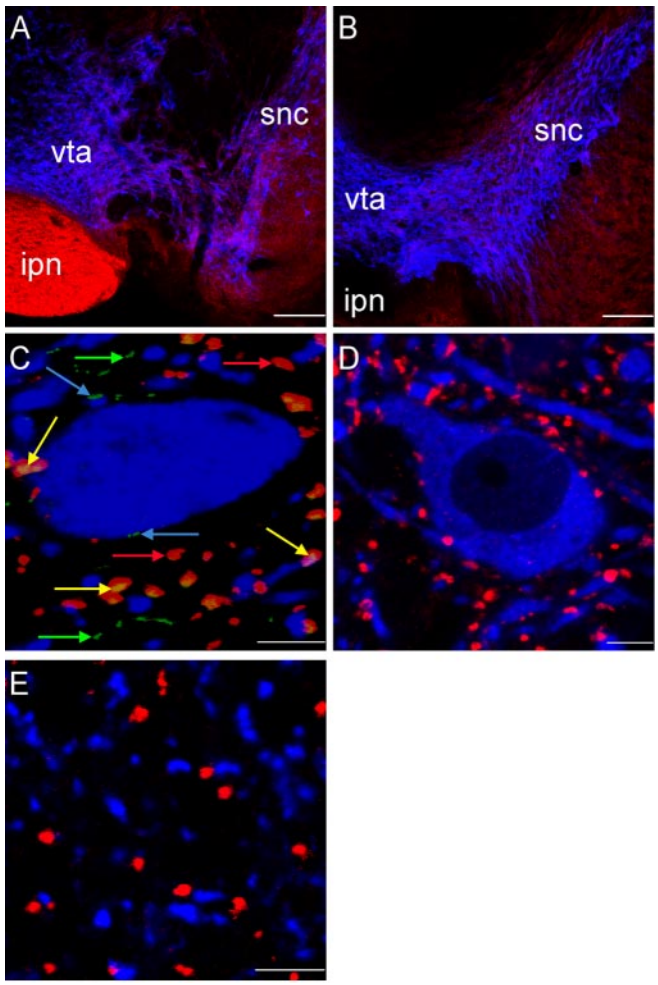

Figure 1. Comparative localization of α7 nAChRs (green), glutamatergic axon terminals (*A–D*, red; *E*, VGluT1, red, VGluT2, blue), and dopaminergic neurons (dendrites and cell bodies, blue) in aldehyde-fixed sections through the adult rat VTA. *A–D*, α7 nAChRs were labeled with Alexa Fluor 488-conjugated αBgt; glutamatergic axon terminals were labeled with anti-VGluT1 or -VGluT2, followed by Alexa Fluor 546-conjugated secondary antibody; dopaminergic neurons were labeled with anti-tyrosine hydroxylase, followed by Alexa Fluor 633-conjugated secondary antibody. *E*, VGluT1 and VGluT2 terminals were labeled with rabbit anti-VGluT1 and guinea pig anti-VGluT2, respectively, followed by Alexa Fluor 546-conjugated anti-rabbit IgG and Alexa Fluor 633-conjugated anti-guinea pig IgG. *A*, *B*, Low-magnification images of VGluT1 (*A*) and VGluT2 (*B*) immunoreactivites in the VTA and surrounding nuclei. VGluT1 labeling is particularly strong in the interpeduncular nucleus (ipn), with moderate levels in the VTA (*A*). In contrast, VGluT2 immunoreactivity is stronger in the VTA but apparently absent from the ipn (*B*). Note that no αBgt signal was detected at this magnification. *C*, Higher-magnification image of the VTA labeled for both VGluT1 and VGluT2. Three populations of αBgt binding sites are revealed, associated with VGluT-immunoreactive axon terminals (yellow arrows), dopaminergic neurons (blue arrows), and nondopaminergic cells (green arrows). Note that not all glutamatergic axon terminals express detectable levels of α7 nAChRs (red arrows). *D*, Competition control, in which preincubation with an excess of unconjugated αBgt obliterated fluorescent αBgt labeling. Note the lack of green and yellow fluorescent spots. *E*, Dual labeling for VGluT1 (rabbit anti-VGluT1, red) and VGluT2 (guinea pig anti-VGluT2, blue) immunoreactivity in the VTA; no detectable colocalization of the two VGluT isoforms within the same structures was observed. snc, Substantia nigra pars compacta. Scale bars: *A*, *B*, 200 μm; *C–E*, 20 μm.

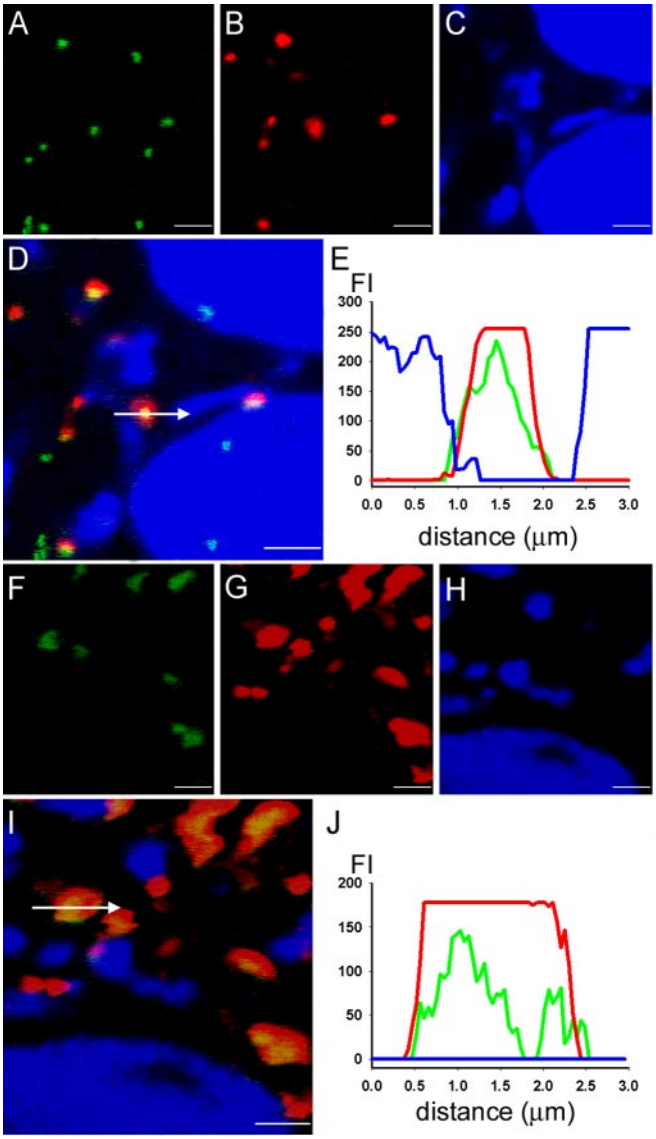

Figure 2. Colocalization of α7 nAChRs and glutamatergic axon terminals in aldehyde-fixed sections through the adult rat VTA. α7 nAChRs were labeled with Alexa Fluor 488-conjugated αBgt (*A*, *F*, green); glutamatergic axon terminals were labeled with anti-VGluT1 (*B*) or anti-VGluT2 (*G*), followed by Alexa Fluor 546-conjugated secondary antibody (red); dopaminergic neurons were labeled with anti-tyrosine hydroxylase, followed by Alexa Fluor 633-conjugated secondary antibody (*C*, *H*, blue). *D*, *I*, Merged images. αBgt binding sites colocalized with both VGluT1-immunopositive (*A–D*) and VGluT2-immunopositive (*F–I*) axon terminals. Fluorescence profile analyses, along the paths indicated by white arrows in *D* and *I*, confirm the colocalization of αBgt with both VGluT1-immunoreactive (*E*) and VGluT2-immunoreactive (*J*) axonal boutons (see Materials and Methods). FI, Fluorescence intensity. Scale bars, 5 μm.

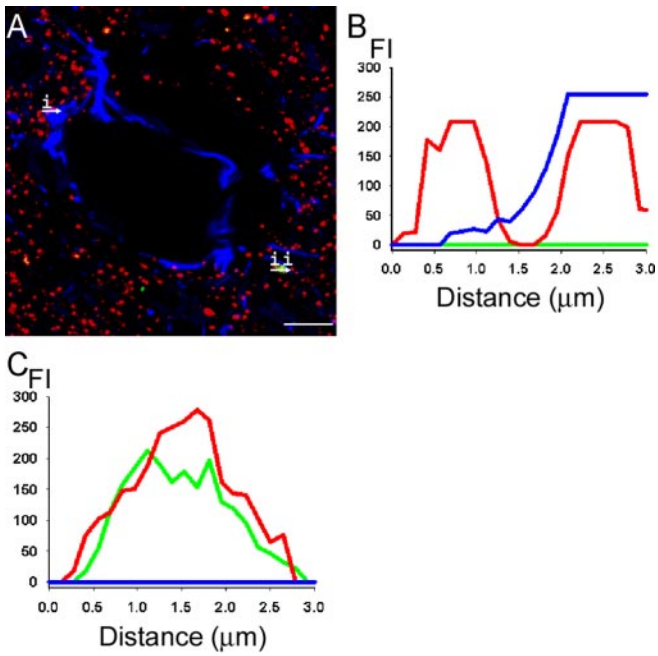

Figure 3. Localization of VGluT immunoreactivity, but not α7 nAChRs, within GFAP-positive astrocytes in aldehyde-fixed sections through the adult rat VTA. α7 nAChRs were labeled with Alexa Fluor 488-conjugated αBgt (green); glutamatergic axon terminals were labeled with anti-VGluT1 and -VGluT2, followed by Alexa Fluor 546-conjugated secondary antibody (red); astrocytes were labeled with anti-GFAP, followed by Alexa Fluor 633-conjugated secondary antibody (blue). *A*, VGluT immunoreactivity was observed within GFAP-positive structures, exemplified in *B* by the fluorescence profile analysis of line i. Note the absence of associated αBgt label. αBgt binding sites also colocalized with glutamatergic axon terminals, exemplified in *C* by the fluorescence profile analysis of line ii. FI, Fluorescence intensity. Scale bars, 10 μm.

dicating colocalization of α7 nAChRs with glutamatergic axon terminals. Profile analysis of 100 VGluT1- and 100 VGluT2-labeled axonal boutons in the VTA revealed that 25% of VGluT1- and 31% of VGluT2-immunoreactive boutons expressed detectable αBgt binding sites. In comparison, similar analyses within the shell of the NAcc from the same rats found that 30% of VGluT1- and 72% of VGluT2-immunoreactive boutons expressed detectable αBgt binding sites.

To address the identity of VGluT-immunoreactive structures in the VTA, we determined whether VGluT is expressed by glial cells, as well as axonal boutons. Aldehyde-fixed sections were triple-labeled with α7 nAChRs, VGluT1 and VGluT2, and GFAP for confocal analysis (Fig. 3*A*). VGluT immunoreactivity was detected within a subpopulation of astrocytic processes within the VTA, and this association was confirmed by fluorescence profile analysis (Fig. 3*B*). Triple labeling, however, failed to demonstrate any expression of α7 nAChRs within VTA astrocytes; in all of the cases examined, αBgt binding sites were restricted to non-GFAP-immunopositive structures, including glutamatergic axon terminals (Fig. 3*C*).

Similar experiments comparing the localization of α7 nAChRs and cholinergic axon terminals (identified by VAChT immunoreactivity) in the VTA failed to find any incidences of colocalization in coronal VTA sections from five adult rats (Fig. 4*A*). Serial optical sections through the VTA (*z*-stacks) were analyzed to check for fluorescent αBgt binding sites around the entire perimeter of the cholinergic axon terminals, again failing to find any instances of colocalization (data not shown). The absence of detectable αBgt binding sites associated with cholinergic axon terminals in the VTA is in contrast to immunolabeled sections of the NAcc shell from the same rats, in which a proportion of αBgt binding sites colocalized with cholinergic axon terminals (Fig. 4*B*, yellow arrows).

Electron microscopy

Both unfixed and aldehyde-fixed sections through the VTA were used to examine the ultrastructural localization of α7 nAChRs in the VTA using αBgt conjugates. nAChRs do not tolerate conventional glutaraldehyde fixation that provides optimum preservation of tissue morphology at the electron microscope level (Jones et al., 2002). Indeed, αBgt binding and anti-nAChR subunit antibody labeling are significantly reduced even at low concentrations (0.1%) of glutaraldehyde (Jones et al., 2002), so other

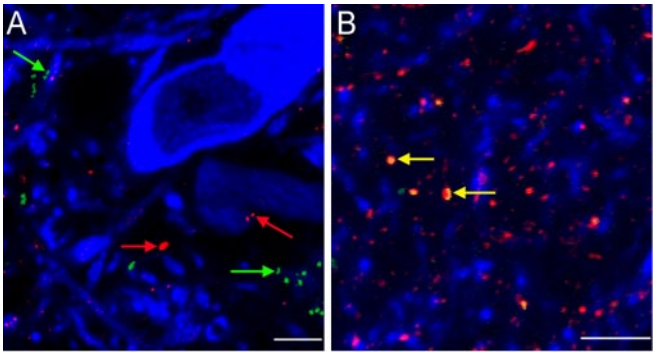

Figure 4. Triple labeling of α7 nAChRs (green), cholinergic axon terminals (red), and dopaminergic dendrites (*A*) or axonal boutons (*B*, blue) in aldehyde-fixed sections through the adult rat VTA (*A*) and NAcc (*B*). α7 nAChRs were labeled with Alexa Fluor 488-conjugated αBgt; cholinergic axon terminals were labeled with anti-VAChT, followed by Alexa Fluor 546-conjugated secondary antibody; dopaminergic neurons were labeled with anti-tyrosine hydroxylase, followed by Alexa Fluor 633-conjugated secondary antibody. In the VTA, α7 nAChRs (green arrows) are located at sites distant from cholinergic axon terminals (red arrows). In contrast, in the NAcc, a subpopulation of αBgt binding sites are associated with VAChT immunoreactivity (yellow arrows). Scale bars, 10 μm.

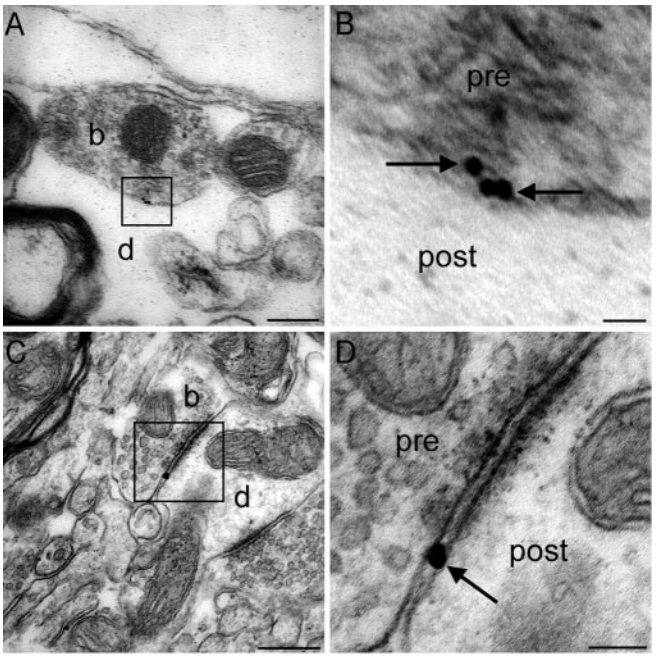

Figure 5. Synaptic localization of α7 nAChRs (arrows) in the adult rat VTA, revealed by labeling of unfixed slices. *A*, Unfixed slice incubated with biotinylated αBgt, followed by postembedding gold labeling for biotin. *B*, Magnified view of the boxed area in *A*, demonstrating the presence of gold particles (arrows) on the plasma membrane of an axonal bouton. *C*, Unfixed slice incubated directly with gold-conjugated αBgt. *D*, Magnified view of the boxed area in *C*, demonstrating the presence of gold particles (arrows) at a perisynaptic locus within a synaptic cleft. The silver reagent has fused the gold particles into a single unit, and, because this is in contact with both the presynaptic and postsynaptic membranes, it is not possible to determine on which membrane the α7 nAChRs are located. Arrows indicate αBgt binding sites. b, Axonal bouton; d, dendrite; pre, presynaptic bouton; post, postsynaptic dendrite. Scale bars: *A–E*, 100 nm; *F*, 150 nm.

strategies were necessary to circumvent this problem. Unfixed sections (Fig. 5) are advantageous, because the receptors are in their native state for labeling and can be postfixed by immersion fixation in glutaraldehyde. However, unfixed sections are incompatible with permeabilization steps, so αBgt penetration is poor and limited to within a few micrometers of the section surface

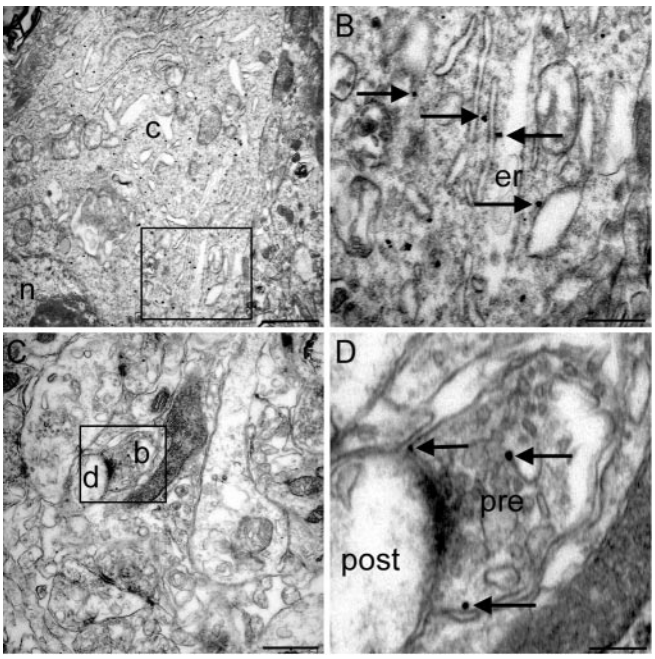

Figure 6. Subcellular localization of α7 nAChRs (some indicated by arrows) in the adult rat VTA, revealed by labeling of aldehyde-fixed sections. *A*, *B*, Sections incubated with biotinylated αBgt, followed by preembedding gold labeling for biotin. *A*, α7 nAChRs within a cell body in the VTA. *B*, Higher magnification of the boxed region in *A* reveals that a proportion of the αBgt binding sites are associated with the endoplasmic reticulum. *C*, *D*, Sections incubated directly with gold-conjugated αBgt. *C*, α7 nAChRs within an axonal bouton in the VTA. *D*, Higher magnification of the boxed region in *C* reveals that αBgt binding sites are located both within the cytoplasm and on the plasma membrane. Arrows indicate αBgt binding sites. b, Axonal bouton; c, cytoplasm; d, dendrite; er, endoplasmic reticulum; n, nucleus; pre, presynaptic bouton; post, postsynaptic dendrite. Scale bars: *A*, *C*, 500 nm; *B*, *D*, 100 nm.

(our unpublished observations). In addition, because cell membrane integrity is maintained, αBgt can bind only to receptors expressed on the cell surface. In this study, optimal tissue preservation was observed within a few micrometers of the section surface, coinciding with the maximal αBgt penetration and binding. In these superficial areas, tissue morphology was poorer than that seen with *in vivo* fixative perfusion, reflecting a combination of postmortem degeneration in ACSF and the slow rate of slice penetration by glutaraldehyde during postlabeling fixation.

Tissue morphology was improved in fixed tissue from brains perfused with PLP fixative *in situ* before sectioning (Fig. 6). This fixative was chosen because it has been shown previously to be a suitable alternative to glutaraldehyde-based fixatives for immunoelectron microscopy studies (McLean and Nakane, 1974). Although morphology is inferior to that seen with glutaraldehyde perfusion *in vivo*, retention of antigenicity is greatly improved. In contrast to unfixed sections, fixed sections are also compatible with detergent permeabilization, revealing both surface and cytoplasmic α7 nAChR populations.

In both unfixed and fixed samples, tissue morphology preservation was sufficient to identify critical cellular structures such as axonal boutons and synapses. At the electron microscope level, assembled α7 nAChRs were precisely localized using two αBgt conjugates, biotinylated and gold-tagged αBgt. Biotinylated αBgt has been used previously to localize α7 nAChRs in the stratum radiatum of the CA1 region of the hippocampus (Fabian-Fine et al., 2001). This conjugate has been shown to be specific for α7 nAChRs, confirmed in this study by competition with excess αBgt or α-cobratoxin, which obliterated labeling (data not

shown) in a manner similar to that of the confocal control experiments (Fig. 1*D*). However, the requirement for a secondary labeling step to detect biotinylated αBgt may be affected adversely by endogenous tissue biotin. For this reason, we have characterized recently a 1.4 nm gold conjugate of αBgt for directly visualizing α7 nAChRs at the light and electron microscope levels (Jones at al., 2004). We showed previously that this conjugate is specific for α7 nAChRs: it displaced [^{3}H]methyllycaconitine binding to rat brain membranes with affinity comparable with that of native αBgt, and PLP-fixed tissue labeling was abolished by preincubation with excess αBgt or α-cobratoxin (Jones et al., 2004).

In unfixed tissue slices through the VTA, α7 nAChRs were localized both on the surface of axon terminals (Fig. 5) and on dendrites themselves (data not shown). No labeling of glial cells, based on morphological criteria, was noted within the VTA. In some instances, the silver enhancement of the gold particle spanned the synaptic cleft, so it is not possible to determine whether the α7 nAChRs are presynaptic or postsynaptic (Fig. 5*D*). There was no apparent difference in labeling with either biotinylated (Fig. 5*A*,*B*) or gold (Fig. 5*C*,*D*) αBgt. Notably, the use of gold-conjugated anti-biotin, in postembedding labeling of epoxy resin-embedded sections to detect biotinylated αBgt, represents a novel technique for identifying receptors; it was mainly used previously to detect amino acids (Ingham, 1992). Interestingly, α7 nAChRs on the surface of axon terminals were rarely seen at active zones of neurotransmitter release and were instead found within the synaptic cleft at the periphery of active zones (perisynaptic loci) (Fig. 5*D*).

Similar results were obtained with PLP-fixed sections, incubated with either biotinylated or gold αBgt (Fig. 6). In these experiments, however, the sections were permeabilized, permitting the visualization of intracellular αBgt binding sites. α7 nAChRs were observed in the cytoplasm of a subpopulation of VTA neurons (Fig. 6*A*,*B*), often associated with the endoplasmic reticulum (Fig. 6*B*). α7 nAChRs were also observed in presynaptic boutons (Fig. 6*C*,*D*). Semiquantitative analysis of gold αBgt labeling in 100 random fields revealed that 57% of α7 nAChRs were somatodendritic, whereas 43% were on axonal boutons within the VTA ($n = 1647$ gold particles). Most α7 nAChRs were cytoplasmic (82% of somatodendritic and 65% of axonal receptors), and the remainder were associated with the plasma membrane (defined as either touching or being within one gold particle diameter distance from the membrane).

In agreement with the unfixed tissue experiments, most gold particles on the surface of axon terminals in contact with dendrites were found at nonsynaptic loci (Fig. 6*D*). Of 140 membrane-associated gold particles, 61% were within the synaptic cleft adjacent to the active zone (perisynaptic), 27% were outside of the synaptic cleft (extrasynaptic), and the remainder (12%) were within the synaptic cleft at the active zone (synaptic).

Many of the axon terminals labeled with biotinylated or gold-conjugated αBgt appear to form asymmetric synapses with dendrites, characteristic of glutamatergic synapses, although the morphological preservation makes this distinction less clear (Figs. 5*C*,*D*, 6*C*,*D*). To determine definitively whether α7 nAChRs are present on glutamatergic axon terminals, as inferred by the confocal results (Fig. 2) and single-labeling studies (Figs. 5*B*,*D*, 6*D*), double-labeling experiments were undertaken at the electron microscope level (Fig. 7). α7 nAChRs were identified using either biotinylated or gold-conjugated αBgt, whereas glutamatergic axon terminals were labeled using anti-VGluT1 or -VGluT2 antibodies and revealed with the DAB reaction product, which forms a dark precipitate visible in electron micrographs. Because gold conjugates of αBgt or anti-biotin IgG do not penetrate sections as efficiently as unconjugated antibodies, analysis was restricted to zones containing gold particles, typically within 10 μm of the section surface. α7 nAChRs were identified in both VGluT1-immunopositive (Fig. 7*A*,*C*) and VGluT2-immunopositive (Fig. 7*B*,*D*) axon terminals in the VTA. In addition to a cytoplasmic location, gold particles were occasionally observed to be associated with the membrane at perisynaptic sites (Fig. 7*A*). Only a subpopulation of glutamatergic axon terminals was found to contain α7 nAChRs (9% of VGluT1 and 11% of VGluT2 terminals; $n = 100$ immunolabeled terminals each). Additionally, when sections were incubated with antibodies to both VGluT1 and VGluT2, a proportion of αBgt binding sites was observed in nonglutamatergic axon terminals (75% associated with either VGluT1 or VGluT2 and 25% associated with unlabeled terminals; $n = 100$ αBgt-labeled axon terminals).

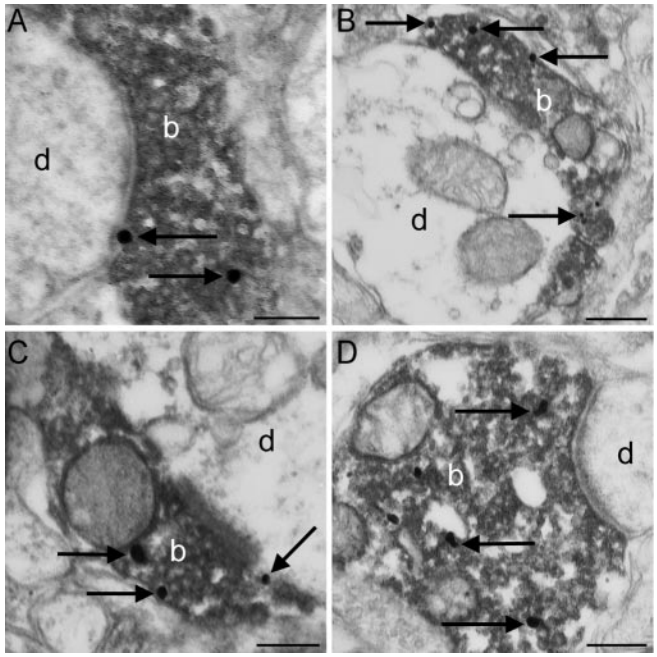

Figure 7. Subcellular localization of α7 nAChRs (some indicated by arrows) in glutamatergic axon terminals (identified by VGluT immunoreactivity and revealed by the DAB reaction product) within aldehyde-fixed sections through the adult rat VTA. *A*, *B*, α7 nAChRs visualized with biotinylated αBgt in VGluT1-immunpositive (*A*) and VGluT2-immunopositive (*B*) axon terminals. *C*, *D*, α7 nAChRs visualized with gold-conjugated αBgt in VGluT1-immunopositive (*C*) and VGluT2-immunopositive (*D*) axon terminals. Arrows indicate αBgt binding sites. b, VGluT-immunoreactive axonal bouton; d, dendrite. Scale bars, 100 nm.

To investigate whether a subpopulation of dopaminergic neurons within the VTA express α7 nAChRs, sections were colabeled with antibodies against tyrosine hydroxylase. Approximately one-half (45%; $n = 30$ neurons) of tyrosine hydroxylase-positive neurons contained gold-conjugated αBgt particles in the VTA. Labeling of α7 nAChRs was observed both in the cytoplasm (Fig. 8*A*,*B*) and on the surface membrane at synaptic sites (Fig. 8*C*) of dopaminergic neurons.

Similar experiments to determine whether α7 nAChRs are present on, or apposed to, cholinergic axonal boutons failed to find any association ($n = 43$ VAChT-immunopositive axonal boutons from 5 rats) (Fig. 8*D*), in agreement with the confocal microscopy results (Fig. 4). As in the latter experiments, serial sections in the *z*-axis were analyzed to check for αBgt binding sites around the whole perimeter of the cholinergic axonal bou-

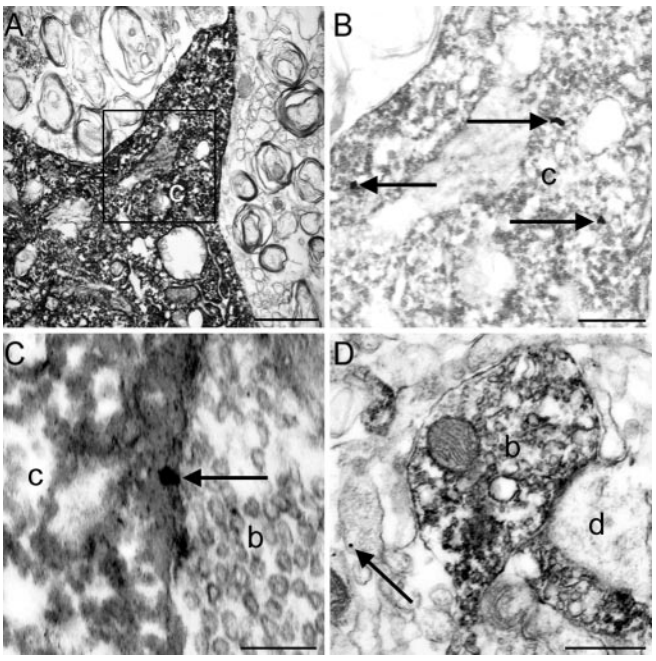

Figure 8. Subcellular relationship between α7 nAChRs and dopaminergic neurons (identified by tyrosine hydroxylase immunoreactivity and revealed by the DAB reaction product; *A–C*) or cholinergic axon terminals (identified by VAChT immunoreactivity and revealed by the DAB reaction product; *D*) within aldehyde-fixed sections through the adult rat VTA. *A*, α7 nAChRs, visualized with gold-conjugated αBgt, within the cytoplasm of a dopaminergic neuron. *B*, High-contrast image of the boxed area in *A*, facilitating visualization of the gold particles. *C*, Postsynaptic α7 nAChRs, visualized with gold-conjugated αBgt, on the plasma membrane of a dopaminergic neuron. *D*, VAChT-immunoreactive axon terminal within the VTA. Note that, although gold-conjugated αBgt labeling is present (arrow), it is not associated with the VAChT-positive terminal. Arrows indicate αBgt binding sites. b, Axonal bouton; c, cytoplasm; d, dendrite. Scale bars: *A*, 500 nm; *B*, *D*, 200 nm; *C*, 100 nm.

tons. To ensure that this lack of association between α7 nAChRs and cholinergic axonal boutons was not attributable to variability in tissue penetration between gold conjugates and antibodies (see above), the presence of gold particles was confirmed at the same level in the section (Fig. 8*D*, arrow).

Discussion

The principal aim of this study was to test the hypothesis that α7 nAChRs reside on glutamatergic axon terminals in the adult rat VTA. Electrophysiological studies have demonstrated previously that the activation of α7 nAChRs enhances glutamatergic signaling within the VTA and can, under certain circumstances, contribute to a form of LTP (Mansvelder and McGehee, 2000; Mansvelder et al., 2002). This relationship is supported by *in vivo* microdialysis studies, which inferred that α7 nAChR-mediated enhancement of glutamate release onto mesolimbic dopaminergic neurons elicited an increase in dopamine release in the NAcc (Schilstrom et al., 1998a,b). Here, we demonstrated that α7 nAChRs are often located on glutamatergic axon terminals at extrasynaptic and perisynaptic sites, whereas cholinergic boutons are not in synaptic contact with presynaptic membranes bearing α7 nAChRs. There was no detectable expression of α7 nAChRs on glial cells in the VTA, although a subpopulation of GFAP-immunopositive astrocytes was found to contain VGluT immunoreactivity.

α7 nAChRs are present on glutamatergic terminals

At the EM level, α7 nAChRs, identified by either biotin- or gold-conjugated αBgt, were found on axon terminals forming synapses onto dendrites (Fig. 5). Morphologically, these synapses often appeared to be asymmetric, consistent with multiple labeling strategies that identified α7 nAChRs on a subpopulation of VGluT-immunoreactive (glutamatergic) terminals. At the cellular level, two populations of glutamatergic synapses in the VTA could be distinguished by their immunoreactivity for either VGluT1 or VGluT2, with VGluT2 predominating (Fig. 1*E*). The lack of colocalization of VGluT1 and VGluT2 immunoreactivities (Fig. 1*E*) indicates that these markers define two populations of glutamatergic synapses. α7 nAChRs were associated with a proportion of both VGluT1- and VGluT2-positive structures. At the confocal microscope level, αBgt binding was associated with 25% of VGluT1- and 31% of VGluT2-immunoreactive boutons. The association was lower at the electron microscope level (9 and 11%, respectively), which may reflect the increased sensitivity of confocal microscopy compared with immunoelectron microscopy. Complementary, nonoverlapping expression of VGluT1 and VGluT2 has been generally observed (Fremeau et al., 2001, 2004; Herzog et al., 2001; Kaneko and Fujiyama, 2002). The significance is unclear, although it has been suggested that VGluT2 is expressed at synapses with a higher probability of glutamate release (Fremeau et al., 2001). VGluT1 mRNA expression predominates in cortical areas, whereas VGluT2 is the predominant transcript in brainstem (Fremeau et al., 2001, 2004; Herzog et al., 2001; Kaneko and Fujiyama, 2002). Tracing studies will be necessary to discover whether the two populations of glutamate terminals recognized in the present study reflect different pathways projecting to the VTA. Although α7 nAChRs were identified in a similar proportion of both populations of glutamatergic terminals, the greater abundance of VGluT2-positive boutons in the VTA means that, numerically, many more α7 nAChRs are associated with these terminals.

Of the presynaptic α7 nAChRs in the VTA, 35% were associated with the plasma membrane, and the remainder were cytoplasmic. Thus, a higher proportion is membrane-associated than observed previously for the distribution of the nAChR β2 subunit immunoreactivity in the dorsal striatum, in which 15% of β2 subunit immunolabeling was membrane-bound in nigrostriatal dopaminergic axon terminals compared with only 3% for the cytoplasmic enzyme tyrosine hydroxylase (Jones et al., 2001). Interestingly, 61% of presynaptic α7 nAChRs were situated within the synaptic cleft at perisynaptic loci, 27% were extrasynaptic (outside of the synaptic cleft), and only 11% were seen at the active zone, opposed to the postsynaptic density. It is unlikely that this is a result of partial accessibility of the synaptic cleft to the αBgt conjugates because both biotinylated αBgt and gold αBgt have been shown previously to bind to synaptic sites in the hippocampus (Fabian-Fine et al., 2001; Jones et al., 2004). The perisynaptic location of α7 nAChRs at the edges of glutamatergic synapses in the VTA places them in an ideal location for modulating glutamatergic transmission via local depolarization and/or increases in intracellular calcium through α7 nAChRs. Perisynaptic loci for α7 nAChRs have also been described in the cerebellum (Caruncho et al., 1997) and hippocampus (Fabian-Fine et al., 2001), using antibodies against the α7 nAChR subunit and biotinylated αBgt.

α7 nAChRs are also associated with nonglutamatergic structures

Not all synaptic boutons in the VTA that were positive for αBgt were double-labeled with VGluT1 or VGluT2 antibodies. Thus, a proportion (25%) of presynaptic αBgt binding sites in the VTA reside on nonglutamatergic axon terminals. These are unlikely to be cholinergic because double labeling with VAChT failed to find

any incidences of α7 nAChRs on cholinergic axonal boutons (Figs. 4*A*, 8*D*). It is possible that αBgt labels a subset of GABAergic axon terminals because 50% of GABAergic neurons in the VTA express α7 nAChRs, as judged by single-cell PCR (Klink et al., 2001), and some of these will be local interneurons with axon terminals in the VTA.

αBgt labeling was also associated with cell bodies and dendrites of both dopaminergic (Figs. 1*C*, 8*A*,*B*) and nondopaminergic (Fig. 1*C*) neurons within the VTA. α7 nAChRs were localized on somatodendritic membranes, as well as in the cytoplasm of these neurons (Fig. 6*A*,*B*); analysis revealed that 82% of αBgt-associated gold particles were cytoplasmic. Within the cytoplasm, αBgt tended to be associated with the endoplasmic reticulum (Fig. 6*B*), possibly reflecting sites of receptor assembly before translocation to the plasma membrane. The presence of α7 nAChRs in dopaminergic neurons is consistent with single-cell PCR analysis (Klink et al., 2001) and with the demonstration of α7 nicotinic responses in midbrain dopaminergic neurons (Pidoplichko et al., 1997; Tsuneki et al., 2000).

αBgt binding was not observed in glial cell bodies or processes (Fig. 3). Originally, VGluT1 and VGluT2 immunoreactivity was not detected in glial cells (Fremeau et al., 2001, 2004), although a recent study has reported low levels of immunoreactivity for both transporters in a proportion of astrocytic processes in the rat hippocampus (Bezzi et al., 2004). Here, we confirm that this is also the case for the VTA because we also detected low levels of VGluT immunoreactivity in a proportion of GFAP-immunopositive astrocytes within this brain region (Fig. 3*B*), but αBgt labeling was never associated with GFAP immunoreactivity. Although astrocytes have been reported to express functional α7 nAChRs (Sharma and Vijayaraghavan, 2001), these studies have been performed on primary cultures and may not reflect the situation in the mature brain.

Cholinergic innervation in relation to α7 nAChRs

The second major objective of this study was to ascertain the physical relationship between α7 nAChRs and sites of ACh release. Confocal microscopy provided no evidence for the coincidence of fluorescent αBgt and cholinergic axon terminals identified by VAChT immunoreactivity in VTA sections from five rats (Fig. 4*A*). This was verified at the EM level, at which the juxtaposition of VAChT-positive boutons and axon terminals labeled by αBgt was never observed, despite being present in the same field (Fig. 8*D*). Thus, α7 nAChRs are in the vicinity of, but not opposed to, cholinergic axonal boutons. Indeed, VAChT-immunoreactive boutons were only observed in synaptic contact with dendrites in the VTA. Although these results do not preclude the rare occurrence of axoaxonic cholinergic synapses onto glutamatergic terminals in the VTA, they are compatible with other studies indicating that cholinergic afferents from the pedunculopontine tegmental nucleus synapse directly onto the somatodendritic membranes of local GABAergic interneurons and, to a lesser extent, onto dopaminergic neurons in the VTA and do not make axoaxonic synapses (Garzon et al., 1999). The lack of axoaxonic synapses is consistent with a paracrine mode of cholinergic signaling (Descarries et al., 1997; Zoli et al., 1999; Zoli, 2000) to activate presynaptic α7 nAChRs in the VTA. Indeed, the ability of α7 nAChRs to respond to choline, as well as to ACh (Alkondon et al., 1997), adds additional significance to diffuse or volume transmission for the physiological functioning of these receptors and may be pertinent to the involvement of cholinergic nicotinic mechanisms in brain reward systems (Ikemoto and Wise, 2002; Schoffelmeer et al., 2002; Fagen et al., 2003). The EC_{50} values of ACh and choline estimated to activate α7 nAChRs (for example, 130 μM and 1.6 mM, respectively, in rat hippocampal neurons) (Alkondon et al., 1997) greatly exceed ambient levels likely to be in the low micromolar range (Descarries et al., 1997). This raises the question of whether α7 nAChRs would be desensitized rather than activated under such conditions. Functional measurements *in vivo* will be necessary to evaluate this relationship.

In summary, this study provides direct neuroanatomical evidence for presynaptic α7 nAChRs on a subset of glutamatergic axon terminals in the VTA. These receptors are strategically placed to enhance the release of glutamate onto dopaminergic neurons. The absence of direct cholinergic synaptic input to presynaptic α7 nAChRs indicates that these receptors are likely to be activated by endogenous ACh or choline diffusing from local cholinergic terminals. This insight into the neuroanatomical relationships in the VTA is relevant for the emerging role of the cholinergic input in reward in general, as well as for the specific mediation of the reinforcing properties of nicotine.

References

Alkondon M, Rocha ES, Maelicke A, Albuquerque EX (1996) Diversity of nicotinic acetylcholine receptors in rat brain. V. α-Bungarotoxin-sensitive nicotinic receptors in olfactory bulb neurons and presynaptic modulation of glutamate release. J Pharmacol Exp Ther 278:1460–1471.

Alkondon M, Pereira EF, Cortes WS, Maelicke A, Albuquerque EX (1997) Choline is a selective agonist of α7 nicotinic acetylcholine receptors in the rat brain neurons. Eur J Neurosci 9:2734–2742.

Aramakis VB, Metherate R (1998) Nicotine selectively enhances NMDA receptor-mediated synaptic transmission during postnatal development in sensory neocortex. J Neurosci 18:8485–8495.

Bezzi P, Gundersen V, Galbete JL, Seifert G, Steinhauser C, Pilati E, Volterra A (2004) Astrocytes contain a vesicular compartment that is competent for regulated exocytosis of glutamate. Nat Neurosci 7:613–620.

Caruncho HJ, Guidotti A, Lindstrom J, Costa E, Pesold C (1997) Subcellular localization of the α7 nicotinic receptor in rat cerebellar granule cell layer. NeuroReport 8:1431–1433.

Corrigall WA, Franklin KB, Coen KM, Clarke PB (1992) The mesolimbic dopaminergic system is implicated in the reinforcing effects of nicotine. Psychopharmacology 107:285–289.

Dajas-Bailador F, Wonnacott S (2004) Nicotinic acetylcholine receptors and the regulation of neuronal signalling. Trends Pharmacol Sci 25:317–324.

Descarries L, Gisiger V, Steriade M (1997) Diffuse transmission by acetylcholine in the CNS. Prog Neurobiol 53:603–625.

Engelman HS, MacDermott AB (2004) Presynaptic ionotropic receptors and control of transmitter release. Nat Rev Neurosci 5:135–145.

Fabian-Fine R, Skehel P, Errington ML, Davies HA, Sher E, Stewart MG, Fine A (2001) Ultrastructural distribution of the α7 nicotinic acetylcholine receptor subunit in rat hippocampus. J Neurosci 21:7993–8003.

Fagen ZM, Mansvelder HD, Keath JR, McGehee DS (2003) Short- and long-term modulation of synaptic inputs to brain reward areas by nicotine. Ann NY Acad Sci 1003:185–195.

Fremeau RT, Troyer MD, Pahner I, Nygaard GO, Tran CH, Reimer RJ, Bellocchio EE, Fortin D, Storm-Mathisen J, Edwards RH (2001) The expression of vesicular glutamate transporters defines two classes of excitatory synapse. Neuron 31:247–260.

Fremeau RT, Voglmaier S, Seal RP, Edwards RH (2004) VGLUTs define subsets of excitatory neurons and suggest novel roles for glutamate. Trends Neurosci 27:98–103.

Fucile S (2004) Ca^{2+} permeability of nicotinic acetylcholine receptors. Cell Calcium 35:1–8.

Garzon M, Vaughan RA, Uhl GR, Kuhar MJ, Pickel VM (1999) Cholinergic axon terminals in the ventral tegmental area target a subpopulation of neurons expressing low levels of the dopamine transporter. J Comp Neurol 410:197–210.

Gerrits MA, Van Ree JM (1996) Effect of nucleus accumbens dopamine depletion on motivational aspects involved in initiation of cocaine and heroin self-administration in rats. Brain Res 713:114–124.

Gray R, Rajan AS, Radcliffe KA, Yakehiro M, Dani JA (1996) Hippocampal synaptic transmission enhanced by low concentrations of nicotine. Nature 383:713–716.

Herber DL, Severance EG, Cuevas J, Morgan D, Gordon MN (2004) Biochemical and histochemical evidence of nonspecific binding of alpha7nAChR antibodies to mouse brain tissue. J Histochem Cytochem 52:1367–1376.

Herzog E, Bellenchi GC, Gras C, Bernard V, Ravassard P, Bedet C, Gasnier B, Giros B, El Mestikawy S (2001) The existence of a second vesicular glutamate transporter specifies subpopulations of glutamatergic neurons. J Neurosci 21:RC181(1–6).

Ikemoto S, Wise RA (2002) Rewarding effects of the cholinergic agents carbachol and neostigmine in the posterior ventral tegmental area. J Neurosci 22:9895–9904.

Ingham CA (1992) Immunocytochemistry II: post-embedding staining. In: Experimental neuroanatomy, a practical approach (Bolam JP, ed), pp 129–151. Oxford: IRL.

Jones IW, Bolam JP, Wonnacott S (2001) Presynaptic localisation of the nicotinic acetylcholine receptor β2 subunit immunoreactivity in rat nigro-striatal dopaminergic neurons. J Comp Neurol 439:234–247.

Jones IW, Bolam JP, Wonnacott S (2002) Localisation of neuronal nicotinic acetylcholine receptor subunits in rat substantia nigra and dorsal striatum. Adv Behav Biol 52:127–137.

Jones IW, Barik J, O'Neill MJ, Wonnacott S (2004) α Bungarotoxin-1.4 nm gold: a novel conjugate for visualising the precise subcellular distribution of α7* nicotinic acetylcholine receptors. J Neurosci Methods 134:65–74.

Kaneko T, Fujiyama F (2002) Complementary distribution of vesicular glutamate transporters in the central nervous system. Neurosci Res 42:243–250.

Kawai H, Zago W, Berg DK (2002) Nicotinic α7 receptor clusters on hippocampal GABAergic neurons: regulation by synaptic activity and neurotrophins. J Neurosci 22:7903–7912.

Klink R, d'Exaerde AA, Zoli M, Changeux JP (2001) Molecular and physiological diversity of nicotinic acetylcholine receptors in the midbrain dopaminergic nuclei. J Neurosci 21:1452–1463.

Mansvelder HD, McGehee DS (2000) Long-term potentiation of excitatory inputs to brain reward areas by nicotine. Neuron 27:349–357.

Mansvelder HD, Keath JR, McGehee DS (2002) Synaptic mechanisms underlie nicotine-induced excitability of brain reward areas. Neuron 33:905–919.

McLean IW, Nakane PK (1974) Periodate-lysine-paraformaldehyde fixative. A new fixation for immunoelectron microscopy. J Histochem Cytochem 22:1077–1083.

Oakman SA, Faris PL, Kerr PE, Cozzari C, Hartman BK (1995) Distribution of pontomesencephalic cholinergic neurons projecting to substantia nigra differs significantly from those projecting to ventral tegmental area. J Neurosci 15:5859–5869.

Pidoplichko VI, DeBiasi M, Williams JT, Dani JA (1997) Nicotine activates and desensitizes midbrain dopamine neurons. Nature 390:401–404.

Rassnick S, Stinus L, Koob GF (1993) The effects of 6-hydroxydopamine lesions of the nucleus accumbens and the mesolimbic dopamine system on oral self-administration of ethanol in the rat. Brain Res 623:16–24.

Robbins TW, Everitt BJ (2002) Limbic-striatal memory systems and drug addiction. Neurobiol Learn Mem 78:625–636.

Schilstrom B, Nomikos GG, Nisell M, Hertel P, Svensson TH (1998a) *N*-Methyl-D-aspartate receptor antagonism in the ventral tegmental area diminishes the systemic nicotine-induced dopamine release in the nucleus accumbens. Neuroscience 82:781–789.

Schilstrom B, Svensson HM, Svensson TH, Nomikos GG (1998b) Nicotine and food induced dopamine release in the nucleus accumbens of the rat: putative role of α7 nicotinic receptors in the ventral tegmental area. Neuroscience 85:1005–1009.

Schoffelmeer AN, De Vries TJ, Wardeh G, Van de Ven HW, Vanderschuren LJ (2002) Psychostimulant-induced behavioral sensitization depends on nicotinic receptor activation. J Neurosci 22:3269–3276.

Seguela P, Wadiche J, Dineley-Miller K, Dani JA, Patrick JW (1993) Molecular cloning, functional properties, and distribution of rat brain α7: a nicotinic cation channel highly permeable to calcium. J Neurosci 13:596–604.

Sharma G, Vijayaraghavan S (2001) Nicotinic cholinergic signaling in hippocampal astrocytes involves calcium-induced calcium release from intracellular stores. Proc Natl Acad Sci USA 98:4148–4153.

Tsuneki H, Klink R, Lena C, Korn H, Changeux JP (2000) Calcium mobilization elicited by two types of nicotinic acetylcholine receptors in mouse substantia nigra pars compacta. Eur J Neurosci 12:2475–2485.

Wise RA, Rompre PP (1989) Brain dopamine and reward. Annu Rev Psychol 40:191–225.

Zoli M (2000) Distribution of cholinergic neurons in the mammalian brain with special reference to their relationship with neuronal nicotinic acetylcholine receptors. In: Neuronal nicotinic receptors (Clementi F, Fornasari D, Gotti C, eds), pp 13–26. Berlin: Springer.

Zoli M, Jansson A, Sykova E, Agnati LF, Fuxe K (1999) Volume transmission in the CNS and its relevance for neuropsychopharmacology. Trends Pharmacol Sci 20:142–150.